THE JOURNAL OF PHYSICAL CHEMISTRY C

Article

pubs.acs.org/JPCC

Metalation of Porphyrins by Lanthanide Atoms at Interfaces: Direct Observation and Stimulation of Cerium Coordination to 2H-TPP/Ag(111)

Felix Bischoff,[†] Knud Seufert,[†] Willi Auwärter,*[,†] Ari P. Seitsonen,[‡] Daniel Heim,[†] and Johannes V. Barth[†]

[†]Physik-Department E20, Technische Universität München, James Franck Straße 1, D-85748 Garching, Germany

[‡]Département de Chimie, Ecole Normale Supérieure, Sorbonne Université, Centre National de la Recherche Scientifique, 24 rue Lhomond, F-75005 Paris, France

Supporting Information

ABSTRACT: Although on-surface metalation protocols of tetrapyrroles with 3*d* metals are well established, reports on the formation of lanthanide tetrapyrrole complexes are scarce. Here, we address the synthesis of lanthanide-tetrapyrrole units in detail, refining earlier findings. Specifically, the formation of cerium tetraphenylporphyrin (Ce-TPP) was induced on Ag(111) either by thermal annealing or by a manipulation procedure using a scanning tunneling microscope (STM) tip. While the self-assembled TPP arrays are not altered upon Ce metalation, our STM observations show distinct modifications of submolecular features reflecting a multistep reaction pathway. The metalation proceeds from an initial configuration with a 2H-TPP molecule sitting atop a Ce atom via an intermediate state, where the macrocycle is partially deprotonated, to metalated Ce-TPP. The hitherto elusive 1H species state—hypothesized in several 3d metalation studies—is visualized directly. Our study provides novel insights into the on-surface synthesis of tetrapyrroles and lanthanide-based nanosystems.

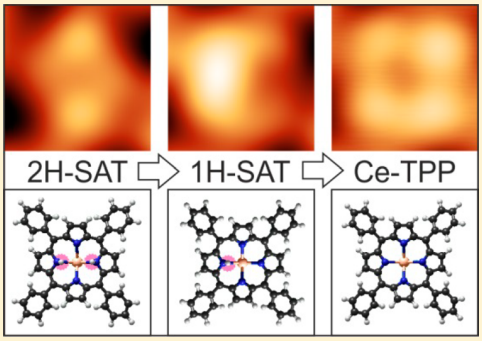

INTRODUCTION

On-surface tetrapyrrole metalation protocols under ultrahigh vacuum (UHV) have been established as versatile approaches for the engineering of metal-organic complexes and nanostructures that cannot be easily achieved on surfaces by standard preparation techniques.[1−4] The considerable research efforts are motivated by the potential for applications of metallotetrapyrroles in photovoltaics,[5,6] catalysis,[7] sensing[8] and quantum technology, among many others.[9] Since the metal center in the macrocycle has great influence on molecular functionalities, the selection and control over this central ion is essential. While the formation of 3*d* metal tetrapyrrole complexes was intensely studied,[1,2,10,11] reports on the *in situ* incorporation of lanthanide metals are scarce and emphasize sandwich structures where the lanthanide is bound not to one but to two tetrapyrroles[12] and thin films thereof.[13] Double-deckers or multideckers where 8-fold coordination of lanthanide centers couples two tetrapyrrole macrocycles are of great interest and have been explored for many years.[14,15] They can notably act as field-effect transistors and single-molecule magnets,[16−21] in favorable situations preserving their properties even on metallic supports.[22,23] However, to gain a fundamental understanding of the relevant chemical processes during on-surface metalation and to tackle surface-anchored coordinatively unsaturated lanthanide tetrapyrrole complexes, the investigation of species comprising only one molecular ligand is desirable. Solution-based approaches and theoretical studies describe the redox reaction from free-base to metalated molecule as a multistep sequence for transition metals.[24−26] First, the intact macrocycle binds to a metal ion. This precursor state is often referred to as sitting atop (SAT) complex. Subsequently, one hydrogen is removed from the macrocycle to form an intermediate SAT and finally, the metallotetrapyrrole evolves under release of H_2. This theoretically suggested reaction pathway has been experimentally corroborated by observing the precursor in solution[27] as well as at the solid−vacuum interface.[28−31] To date a clear experimental proof is still lacking for the intermediate SAT.

Herein, we report a low-temperature (LT) STM and scanning tunneling spectroscopy (STS) study on intermediate complexes formed during the metalation of tetrapyrroles with lanthanide atoms, complemented by extensive density functional theory (DFT) calculations. Specifically, we use free-base 5,10,15,20-tetraphenylporphyrin (2H-TPP) molecules and Ce deposited sequentially on Ag(111). Both annealing and STM tip manipulations trigger the stepwise metalation reaction from

Received: October 19, 2017
Revised: January 28, 2018

DOI: 10.1021/acs.jpcc.7b10363
J. Phys. Chem. C XXXX, XXX, XXX−XXX

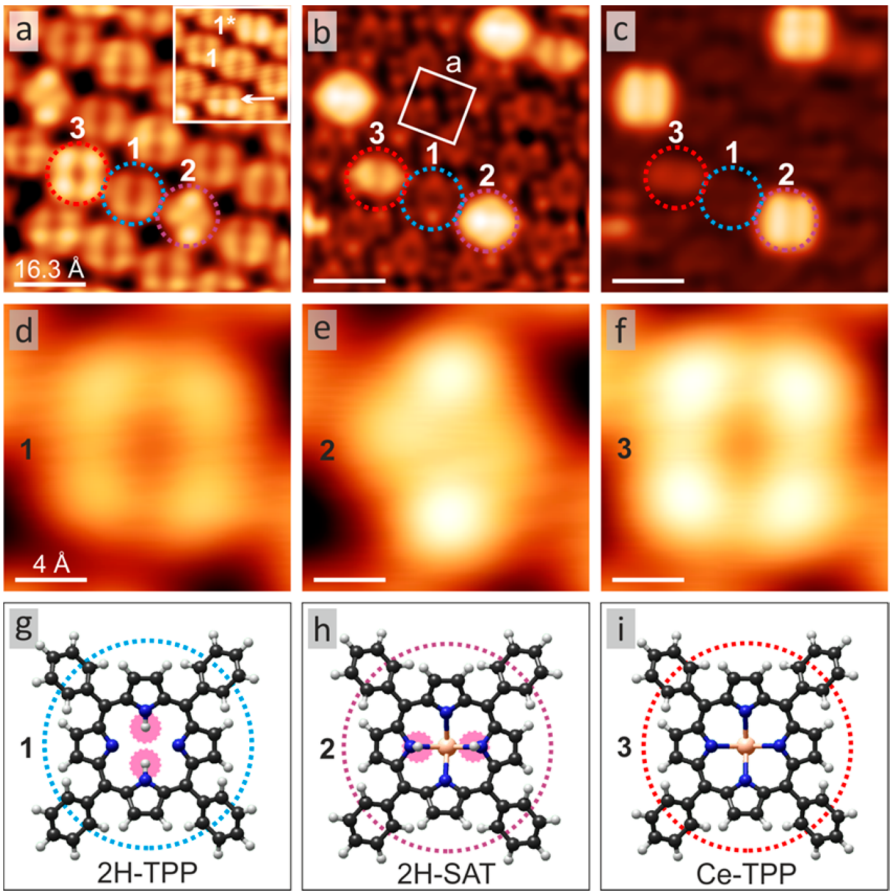

Figure 1. STM characterization of Ce-induced conversions within TPP arrays (measured with (a) U = 1.25 V, (b) U = −0.05 V, and (c) U = −1.25 V; all images of the same area, the white square in part b) highlights the TPP/Ag(111) unit cell with side length a = 1.4 nm). At 1.25 V the three prevalent species **1**−**3** exhibit a similar apparent height and are easy to distinguish. **1** is 2H-TPP (blue), **2** a precursor sitting atop complex with a cerium atom underneath the tetrapyrrole macrocycle (purple) and **3** the metalated Ce-TPP following hydrogen abstraction (red). The inset in part a depicts the two tautomeric forms **1** and **1*** of 2H-TPP. The white arrow serves as guide to the eye for a scanning induced tautomerization reaction. (d−f) Detailed images of each species at 1.25 V. (g−i) Corresponding illustrative models. In the models, the central hydrogens are highlighted for clarity. The orientation of the models corresponds directly to the STM data shown above and was determined by simulated STM images based on DFT modeling (cf. Figure 5). Scan parameters: (a, d−f) I = 0.20 nA, U = 1.25 V; (b) I = 0.20 nA, U = −0.05 V; (c) I = 0.20 nA, U = −1.25 V.

the precursor 2H-SAT, via the reaction intermediate 1H-SAT to the metalloporphyrin unit. This study covers the complete on-surface synthesis scheme toward formation of Ce-TPP. A theoretical examination of the energetics of the observed species based on DFT modeling including the surface rationalizes the experimental findings and a comparison of simulated STM images helps to identify all involved species. DFT also allows to follow subtle geometric adaptations during the metalation process. Furthermore, we reassess previously published data on the interaction of Ce with porphyrin arrays.[32] Whereas these earlier findings suggested Ce-TPP formation within mixed cobalt (II) tetraphenylporphyrin (Co-TPP) and 2H-TPP precursor layers, they are now associated with a more complex Ce−Co-TPP structure involving 3d−4f metal interactions (see also the related finding of site-specific Fe atoms bonding at adsorbed Co-TPP layers[33]).

METHODS

Scanning Tunneling Microscopy. All STM experiments were performed in a custom-designed UHV system providing a base pressure below 5 × 10^{-10} mbar.[34] All data were acquired employing a low-temperature CreaTec-STM[35] with the sample held at 6 K using electrochemically etched W tips. For imaging the constant-current mode was employed. In the figure captions, U refers to the bias voltage applied to the sample. Models were generated in the framework of the HyperChem 7.5 Software Package. The Gwyddion software was used for the analysis of STM images.[36]

Sample Preparation. The monocrystalline Ag(111) substrate was cleaned by repeated Ar^+ sputtering cycles at an energy of 800 eV, followed by annealing at 730 K for 10 min. The synthesis of mixed 2H-TPP/2H-SAT/Ce-TPP arrays was realized by depositing 2H-TPP (Sigma-Aldrich, purity ≥99%) by organic molecular beam epitaxy from a thoroughly degassed quartz crucible held at 600 K and evaporation of Ce atoms from a homemade water-cooled cell by resistively heating a W filament enclosing a Ce ball of high purity (99.9999%, MaTecK GmbH, D-52428 Jülich, Germany). During deposition, the Ag(111) surface was kept at 373 K. For the control experiment with Co-TPP (Sigma-Aldrich, purity ∼95%), Co-TPP was deposited from a thoroughly degassed quartz crucible held at 630 K. During the growth experiments the pressure remained <5 × 10^{-10} mbar. Regarding coverage, we define one monolayer as a surface fully covered by 2H-TPP species.

Density Functional Theory. We performed total energy calculations using DFT[37] within the Kohn−Sham formalism[38]

DOI: 10.1021/acs.jpcc.7b10363
J. Phys. Chem. C XXXX, XXX, XXX−XXX

using the Quantum ESPRESSO code (http://www.Quantum-ESPRESSO.org/).[39] The rB86-vdW-DF2 approximation[40] to the exchange correlation functional was applied. We used the cutoff energy of 60 and 350 Ry to expand the Kohn−Sham orbitals and the augmented electron density, respectively. The projector-augmented wave data sets were obtained from pslibrary.[41] Γ point was used in the calculations due to the relatively large dimensions, together with the Fermi−Dirac broadening of the occupation numbers with a width of 50 meV. Two molecules were inserted in a$(7 \times 4\sqrt{3})$ unit cell that is close to the experimentally derived periodicity.[42] Five layers of substrate were employed. The computed lattice constant of 4.1075 Å was used in the calculations. The initial structure was constructed following the literature,[42] with the centers of molecules at two hollow sites (one hcp, one fcc site), and subsequently relaxing the geometry. The centers moved upon the relaxation somewhat, but remained at about the same distance from their corresponding 3-fold site. The adsorption energy was defined as the difference in the total energies of the adsorbed complex minus the relaxed clean surface and two times an individual molecule in the gas phase, with the convention of positive adsorption energy indicating attraction. The simulated STM images were obtained using the Tersoff−Hamann method[43] by including the orbital densities of the orbitals from the Fermi energy to the given bias voltage, and using an iso-value (10^{-7} e/a_0^3) of the partial electron density at each lateral point on the density mesh to construct the two-dimensional maps.

EXPERIMENTAL AND THEORETICAL RESULTS

STM and STS Observations. *meso*-Substituted tetraphenylporphyrins (TPP) are known to assemble into extended, well ordered islands on the (111) surface of a silver single crystal.[42,44] Irrespective of the exposure to small amounts of Ce atoms, the molecules retain the pertaining noncommensurate lattice with a square unit cell (1.4 nm x 1.4 nm), marked in white in Figure 1b and Figure S1c. Each molecule is oriented with its main axis along a $\langle 11\bar{2} \rangle$ high symmetry direction of the Ag(111) surface (for details see Supporting Information). At submonolayer coverages, the island formation is mainly driven by attractive T-type interactions between the phenyl meso-substituents.[45] 2H-TPPs appear as described in previous STM studies:[46−48] a donut-shaped macrocycle appears at negative sample bias and at small bias voltages around the Fermi level, while a window-like 4-fold symmetric contrast dominates when probing the unoccupied states (Figure 1 and Figure S1). A 2H-TPP unit is marked by blue dashed circles and is referred to as species **1** in Figure 1. Scanning at elevated bias voltages (|U| > 0.8 V) induces reversible switching of contrast as indicated by the white arrow in the inset in Figure 1a. This reversible transition is assigned to a tautomerization reaction, i.e., the correlated proton transfer inside the macrocycle between the nitrogen atoms.[48−51] Consequently, 2H-TPP can appear as two tautomers **1** and **1***.

After exposing submonolayer 2H-TPP arrays on Ag(111) to an atomic beam of Ce at 330 K, intramolecular changes are discernible in the STM images (Figure 1), whereby the order in the molecular layer is unperturbed. Three different species can be identified: free-base TPP (**1**: 2H-TPP, blue), intact 2H-TPP sitting atop of a single cerium atom (**2**: 2H-SAT, purple) and the metalated Ce-TPP (**3**, red). The detailed reasoning of these assignments is elaborated below, notably in the computational modeling (link to section computational modeling) and discussion sections (*vide infra*). Structure models of the species are depicted in Figure 1g−i. The initial SAT complex can be discriminated by two prominent protrusions along a central axis of the molecule for $U > 1$ V (see Figure 1a,e) and by its increased apparent height for $U < -0.65$ V featuring two elongated lobes (purple circle in Figure 1c). Around the Fermi level, 2H-SAT exhibits the largest apparent height and dominates the image contrast (Figure 1b). Ce-TPP strongly resembles 2H-TPP but shows a larger apparent height ($\Delta z \approx 0.3$ Å) for all voltages (cf. Figure 1d−f). An increased adsorption height is confirmed by DFT simulations for all cerium induced species giving values of 0.28 Å (Ce-TPP), 0.42 Å (2H-SAT) and 0.36 Å for the 1H-SAT identified and discussed below (see also Table 3).

To further characterize the species and elucidate the origin of the different submolecular contrast, STS and dI/dV mapping of prominent electronic contributions were carried out. The results are depicted in Figure 2. A common feature in all spectra is an increased density of states at ≈110 mV (dashed line in Figure 2a) that was observed consistently with different tips and in different preparations (see also Figure S4a). Since it appears at a comparable energy for all species within the same array, it presumably does not reflect a molecular contribution, but rather stems from an up-shifted surface state known for

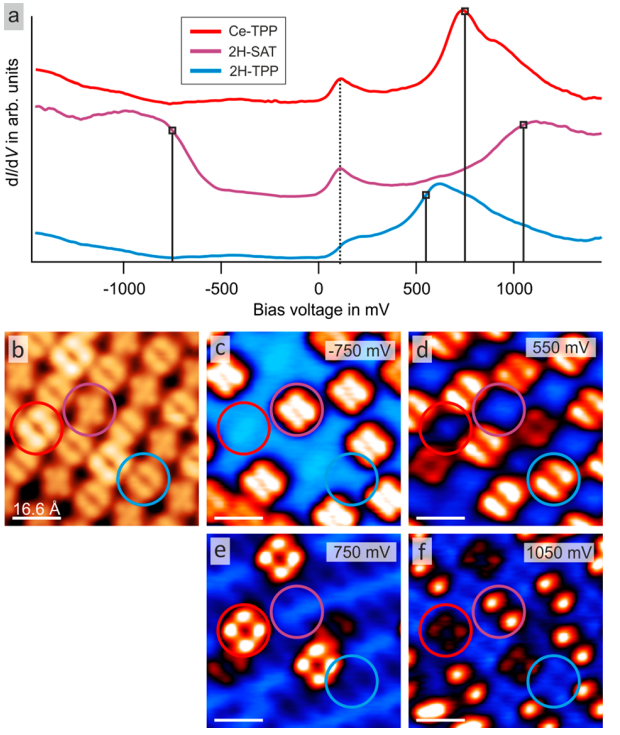

Figure 2. Electronic structure of 2H-TPP and Ce-modified TPP. (a) STS of 2H-TPP, 2H-SAT and Ce-TPP (set point: I = 0.20 nA, U = 1.20 V; color coding of marked species as in Figure 1). The spectra are offset for better comparison and represent averages of multiple measurements acquired above different molecules and positions within an array. Vertical lines mark biases selected for dI/dV mapping in the array whose STM topography is depicted in part b (I = 0.20 nA, U = 1.05 V). (c−f) dI/dV maps of the spatial electron density distribution associated with molecular orbitals of different species: (c) 2H-SAT HOMO, (d) 2H-TPP LUMO, (e) Ce-TPP LUMO, and (f) 2H-SAT LUMO. The bias is indicated in the top right of each map; current set point: I = 0.20 nA.

DOI: 10.1021/acs.jpcc.7b10363
J. Phys. Chem. C XXXX, XXX, XXX−XXX

weakly adsorbed overlayers on transition metal surfaces.[52] The unoccupied region ($U > 0$ V), however, clearly shows distinct molecular features. As expected for 2H-TPP[48,53] (blue curve in Figure 2a), a broad peak from the lowest unoccupied molecular orbital (LUMO) is located slightly above 600 mV.

For the Ce-modified species, the LUMO shifts to higher bias voltages, specifically to ≈1050 mV for 2H-SAT (purple) and ≈750 mV for Ce-TPP (red). In the occupied region ($U < 0$ V), 2H-TPP and Ce-TPP do not exhibit molecular resonances for the probed voltages down to $U = -2000$ mV. By contrast, 2H-SAT features a distinct resonance from the highest occupied molecular orbital (HOMO) at ≈ −750 mV. The dI/dV maps in Figure 2c–f furthermore present the spatial extent of the observed molecular resonances. For comparison, Figure 2b shows an STM image of the same region with highlighted molecules (blue, 2H-TPP; purple, 2H-SAT; red, Ce-TPP). The 2H-TPP LUMO extends as two elongated protrusions, 2-fold symmetrically across the iminic pyrroles, i.e. parallel to the main molecular axis (Figure 2d). In addition, 2H-SAT and Ce-TPP LUMO appear fundamentally different: 2H-SAT shows two prominent protrusions (Figure 2f) located on two opposite macrocyclic pyrroles, while the Ce-TPP appears 4-fold symmetric (Figure 2e). Moreover, it is interesting to note that the 2H-SAT HOMO (Figure 2c) resembles the 2H-TPP LUMO in shape and spatial extent.

In the data set, 2H-SAT and Ce-TPP coexist, which indicates that the employed preparation conditions did either not afford complete conversion before cooling the sample or that 2H-SAT and Ce-TPP are equally favorable in the reaction pathway. The latter option can be disregarded as the yield of fully metalated porphyrins increases substantially following further sample anneal to 390 K for 5 min with a conversion of approximately 90% 2H-SAT into Ce-TPP.

The metalation reaction can also be triggered by scanning at elevated bias and through voltage pulses. Interestingly, such experiments give rise to a new species with only one bright lobe (Figure 3). This species is tentatively assigned to an intermediate SAT complex with a partially deprotonated macrocycle. Accordingly, it is referred to as 1H-SAT, and can be seen as intermediate species between the initial 2H-SAT and the final Ce-TPP product. Indeed, it can finally be transformed to Ce-TPP (cf. Figure 4). Figure 3 depicts the 1H-SAT STM appearance (green circle). It can clearly be discriminated from the other species by scanning at positive and negative sample bias voltages as depicted in Figure 3a,b. For both voltage regimes, 1H-SAT features the distinct off-centered lobe with similar shape. In contrast, the other species change fundamentally when reversing the bias polarity (cf. Figure 1).

A conversion of 2H-SAT via 1H-SAT to Ce-TPP can be induced by applying bias voltages exceeding a threshold of $U \geq 1.4$ V, or $U \leq -1.9$ V. Parts a–c of Figure 4 demonstrate the stepwise, tip-induced metalation by applying a bias of 1.5 V. Below the given voltage the reaction intermediate is stable and can be characterized by STM. Furthermore, the reaction can be directly monitored in the current vs. time trace $I(t)$ of a voltage pulse (Figure 4d). Along the lower trace (green) two steps in the current signal are discernible, while the upper curve (red) only shows one. A comparison of the STM images before and after the pulses thus clearly testifies the formation of Ce-TPP. Therefore, the single step does not correspond to a single deprotonation, but to the full metalation reaction. Note that the deprotonation does not necessarily correspond to a current drop, but can likewise manifest as increase in the magnitude of the tunneling current, depending on the position of the tip above the molecule.

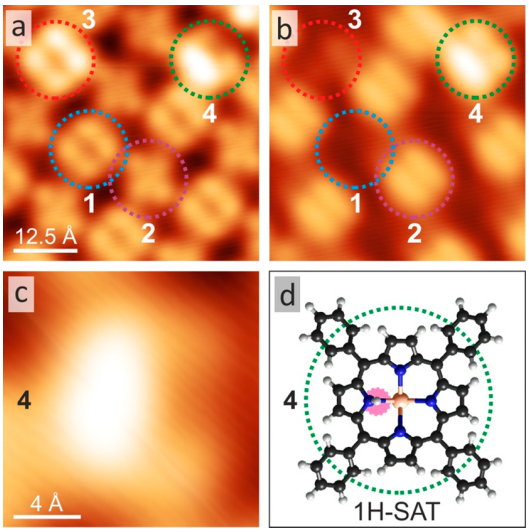

Figure 3. Intermediate Ce–tetrapyrrole complex 1H-SAT. 1H-SAT (**4**, green) appearing markedly different from species **1**–**3**, both at positive (a; $U = 1.00$ V) and negative bias (b; $U = -0.65$ V). It exhibits one bright, off-centered lobe. Upon polarity change, **1**–**3** differ completely in STM data; **4** however remains alike in both voltage regimes. (c) Zoom onto 1H-SAT and (d) corresponding structure model. The orientation of the model corresponds directly to the STM data next to it and was determined by simulated STM images based on DFT modeling (cf. following section). Scan parameters: (a, c) $I = 0.20$ nA, $U = 1.00$ V; (b) $I = 0.20$ nA, $U = -0.65$ V.

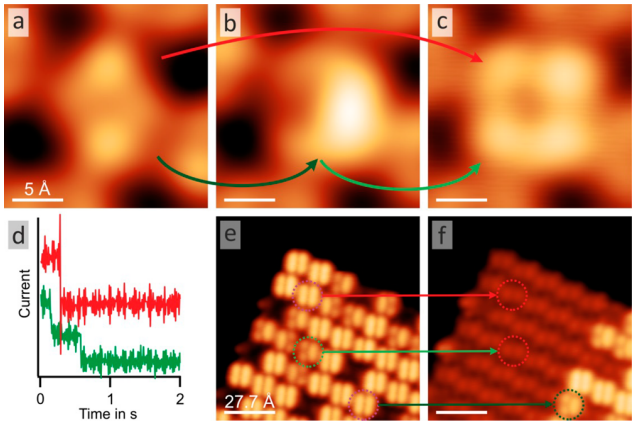

Figure 4. Tip-induced metalation reaction of 2H-TPP with a single Ce atom. (a–c) The precursor complex 2H-SAT (a) is singly deprotonated to form the reaction intermediate 1H-SAT (b) and finally Ce-TPP (c) by applying a voltage of 1.5 V. The red and green arrows depict the reaction pathways observable after tip-interactions. (d) The deprotonation/metalation can be monitored in the current vs time traces of voltage pulses as single (red) and double steps (green, traces vertically offset for clarity). (e, f) Applying a voltage of 2 V at the upper left corner of the array induces transformations of Ce-derived species proceeding simultaneously within the probed area. All possible reaction steps are observable: 2H-SAT to Ce-TPP (top, red), 1H-SAT to Ce-TPP (middle, light green), and 2H-SAT to 1H-SAT (bottom, dark green). Scan parameters: (a–c) $I = 0.20$ nA, $U = 1.20$ V; (e, f) $I = 0.21$ nA, $U = -1.02$ V.

The metalation reaction can be triggered locally with molecular precision when applying pulses close to the threshold

DOI: 10.1021/acs.jpcc.7b10363
J. Phys. Chem. C XXXX, XXX, XXX–XXX

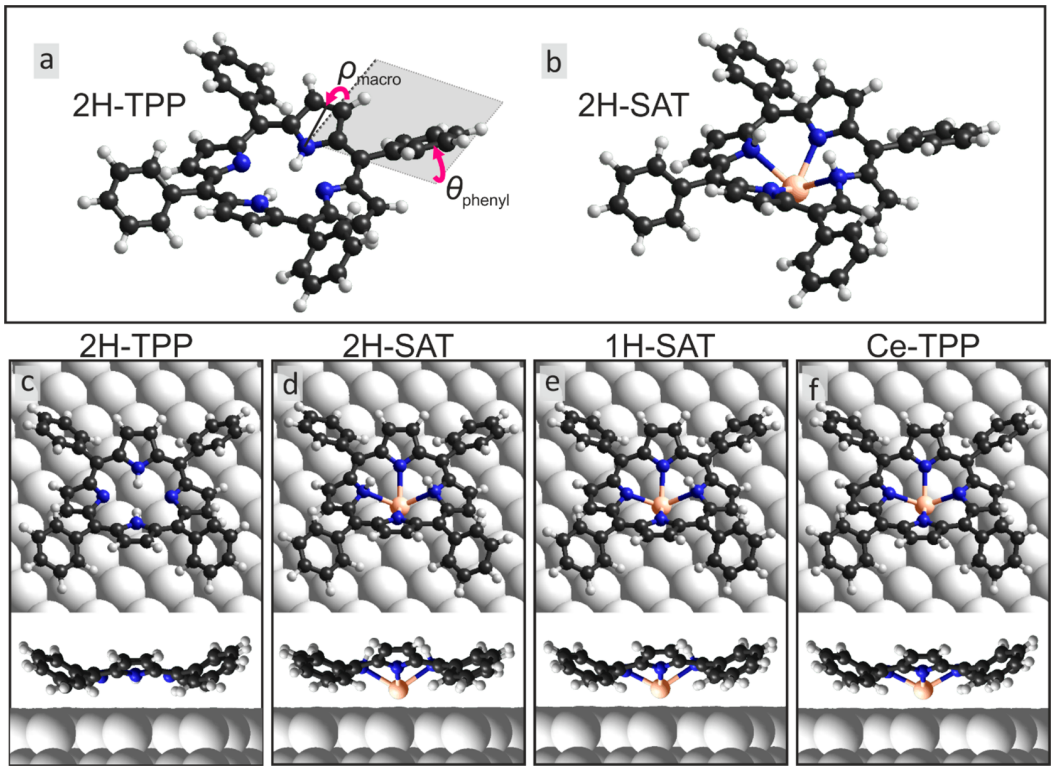

Figure 5. DFT-optimized structure and bonding of free-base, SAT and metalated TPP species on Ag(111). In part a, the macrocycle distortions and phenyl substituent rotational degree of freedom are indicated. The perspective view of the 2H-SAT complex in part b visualizes intramolecular distortions and placement of protons. Parts c–f display top and side views of educt, product, and SAT intermediate species.

value. Moreover, it can be induced over a large area with increased bias voltage. The specific reaction trigger however remains elusive and was not investigated systematically. Figure 4e,f demonstrate the simultaneous metalation of more than 25 molecules within a molecular SAT array by applying 2 V at the top left corner of the island. The observed reactions include all possible reaction steps indicated by arrows in Figure 3e,f: 2H-SAT to Ce-TPP (red, top), 1H-SAT to Ce-TPP (bright green, middle), and 2H-SAT to 1H-SAT (dark green, bottom).

Computational Modeling. To rationalize the experimental findings, we performed total energy calculations using DFT within the Kohn–Sham formalism. The calculations were carried out on a $(7 \times 4\sqrt{3})$ unit cell with two molecules per unit cell (cf. Figure S2). A visual overview of the results and terminology is provided by the models depicted in Figure 5.

Tables 1 and 2 summarize the relevant energetics. Table 1 gives the adsorption energies of the two 2H-TPP tautomers as well as the two possible Ce-TPP adsorption configurations. As expected from tautomerization experiments,[48,51,54] the tautomers are close in energy ($\Delta E \sim 80$ meV). In Ce-TPP, the cerium atom cannot be simply incorporated into the macrocycle plane due to the relatively large size of the metal ion, substantially exceeding atomic diameters of transition metals.[32] This results in two possible interfacial bonding configurations: either with the cerium atom pointing toward the surface (Ce down) or away from it (Ce up) relative to the molecular plane/macrocycle. From STM and STS data, the orientation cannot be unambiguously identified, although most findings support the Ce down situation (see below). Also the adsorption energies obtained from DFT optimized structures clearly favor Ce down with 5.09 eV/molecule compared to 3.46 eV/molecule for Ce up and therefore substantiate considerations based on experimental data.

Table 2 contains binding energies of the precursor and intermediate SAT complexes. The binding energies represent

Table 1. Adsorption Energies of 2H-TPP and Ce-TPP Species from DFT Calculations[a]

species	adsorption energy E_{ads} (eV/molecule)
2H-TPP, tautomer **1**	**3.22**
2H-TPP, tautomer **1*** (hydrogens rotated 90°)	3.14
Ce-TPP, Ce down	**5.09**
Ce-TPP, Ce up	3.46

[a]For 2H-TPP both tautomers were calculated, for Ce-TPP the two possible configurations for the cerium position above (Ce up) and below (Ce down) the macrocycle plane. Bold values are energetically favored.

Table 2. Binding Energy of Hydrogen Atoms in 2H-SAT and 1H-SAT[a]

species	binding energy E_{bind} (eV/H)
2H-SAT	−0.46
2H-SAT, hydrogens rotated	**−0.07**
1H-SAT	−0.51
1H-SAT, hydrogen rotated	**−0.13**

[a]The energy is always calculated with respect to Ce-TPP/Ag(111) and the hydrogen atoms in H_2 in the gas phase. The positions of the hydrogen atoms correspond to 2H-TPP tautomer **1** for 2H-SAT and to tautomer **1*** for 2H-SAT with rotated hydrogens. Bold values are energetically favored.

DOI: 10.1021/acs.jpcc.7b10363
J. Phys. Chem. C XXXX, XXX, XXX–XXX

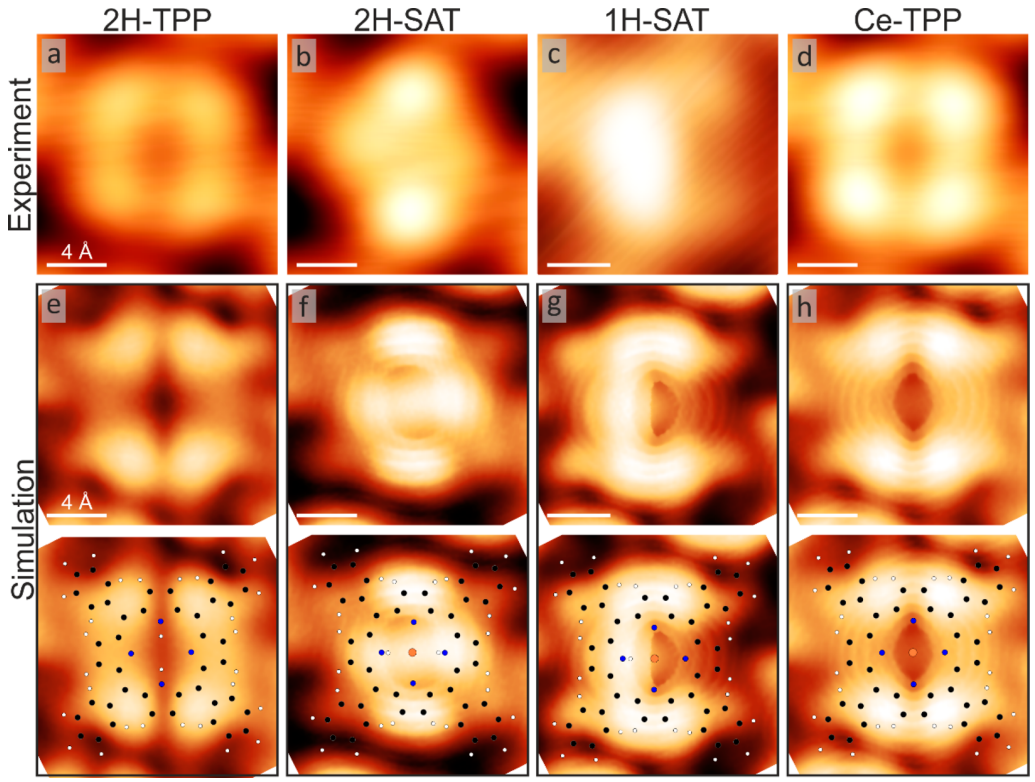

Figure 6. Comparison of experimental with simulated STM data. The first row (a–d) shows the topography of each species as indicated above each column. In parts e–h, the corresponding STM image simulations are reproduced, whereby the lower panels include the atomic positions. Bias voltages for simulations were chosen according to the STM experiments, i.e., 1.25 (a, b, d) and 1.0 V (c).

Table 3. Geometric Parameters Extracted from DFT Optimized Adsorption Geometries[a]

	2H-TPP	2H-SAT	1H-SAT	Ce-TPP (Ce-down)	2H-TPP (gas phase)	Ce-TPP (gas phase)
θ_{phenyl} (deg)	29	33	33	32	61	60
ρ_{macro} (deg)	−14, 21	−21, 28	−17, 26	−14, 24	−6, 6	−5, 15
$\Delta z_{Ce\text{-}mc}$ (Å)	–	−1.37	−1.30	−1.19		0.10
Δz_{mc} (Å)	3.51	3.93	3.87	3.79		
$\Delta z_{Ce\text{-}s}$ (Å)	–	2.56	2.57	2.60		

[a] θ_{phenyl} is the dihedral angle of the phenyl groups, where 0 means a planar alignment, i.e. parallel to the macrocycle plane. ρ_{macro} is the tilt of the pyrrole groups from the macrocycle plane, where 0 means planar. The two values each give the average over the two pyrroles with alike orientation (bending up- or downward, i.e. the nitrogen pointing towards the surface or away from it). While the pyrrole tilt agrees reasonably well with experimental values extracted from NEXAFS,[48] the dihedral angle of the phenyl groups is lower than the reported one, which might be attributed to packing effects. $\Delta z_{Ce\text{-}mc}$ is the height of Ce above (+) or below (−) the macrocycle. Δz_{mc} is the height of macrocycle above the first substrate layer. $\Delta z_{Ce\text{-}s}$ is the height of Ce above the first substrate layer.

relative values compared to Ce-TPP/Ag(111) and hydrogen as gas phase H_2. All these energies are negative, meaning that the ground state is indeed the desorbed H_2 and Ce-TPP/Ag(111), or that 2H–Ce-TPP/Ag(111) (2H-SAT) and H–Ce-TPP/Ag(111) (1H-SAT) are metastable states. Furthermore, the binding energies for SAT tautomers were calculated. Surprisingly, for both SAT species, the rotated tautomer configurations 1*—not favored for 2H-TPP—are preferred by ∼400 meV/H. Consequently, according to our DFT results, the hydrogen positions should change with the evolution of the Ce-tetrapyrrole coordination sphere. A rotation of the whole molecule "on top" of the cerium atom seems unlikely, because of the good agreement of simulated STM images of DFT geometries of tautomer **1*** configurations with experimental data (see below). Furthermore, the incorporation of the molecules into organic arrays results in interlocking of the peripheral phenyls hindering rotational motion, which is supported by STM manipulation experiments at $Ce(TPP)_2$ double and $Ce_2(TPP)_3$ triple deckers.[12] The rotation of TPP moieties is blocked in densely packed $Ce(TPP)_2$ arrays and only possible for the topmost TPP of $Ce_2(TPP)_3$ without direct neighbors protruding from lower layers.

For the energetically favored species, simulated STM images were generated. Figure 6 presents a comparison of the simulation to experimental data for each species, whereby key characteristics nicely match. 2H-TPP and Ce-TPP appear alike exhibiting four lobes. Furthermore, the larger apparent height of Ce-TPP with respect to 2H-TPP is reproduced qualitatively (cf. Figure 6a,e to Figure 6d,h). The good agreement allows in particular the determination of molecular species and molecular features for 2H-SAT and 1H-SAT. In STM, 2H-SAT features two prominent lobes defining a main axis. Close to the middle of the main axis two dimmer lobes are located at the left and right (also compare species **2** in Figure 3a and Figure 4a)

DOI: 10.1021/acs.jpcc.7b10363
J. Phys. Chem. C XXXX, XXX, XXX–XXX

forming a cross-like appearance with a longer side along the main axis. The simulated images express very similar features allowing the assumption that the inner hydrogens of 2H-SAT are situated at different nitrogen atoms compared to 2H-TPP. The prominent lobes in 2H-SAT are observed at the upward bent pyrroles of the TPP macrocycle (i.e., the outer C−C bond is highest and the nitrogens point toward the surface) and do not correspond to the hydrogen positions. This stands in contrast to TPP/Ag(111) where protrusions are a unique signature of the hydrogen positions in 2H-TPP/Ag(111) and 1H-TPP/Ag(111).[48] Nevertheless, the two dimmer lobes do coincide with the hydrogen binding sites and could be related to an electronic effect. 1H-SAT adopts a C-like shape in STM. This asymmetry is reproduced in the simulations as a uniformly appearing C-shape. Note that there is an additional bright protrusion on the C in STM data at the hydrogen position. It remains unclear whether this feature is an electronic effect caused by H-binding since it is not reproduced theoretically.

A geometric effect due to molecular tilting on top of the cerium atom in 1H-SAT cannot be ruled out. Although an evaluation of DFT data for macrocycle tilts only gave angles ≤2.5°, the absolute height difference of the N−H nitrogen and the opposing N amounts to $\Delta z_{\text{NH-N}}$ = 0.18 Å, thus enough to cause considerable changes in the tunneling current.

Table 3 shows geometric parameters for all species that allow following conformational changes induced by the interaction with cerium (angles defined as in Figure 5). Generally, when describing tilt angles of molecular moieties within TPP, a correlation of the pyrrole and phenyl tilts is established that is determined by steric constraints. In gas phase the 2H-TPP macrocycle is almost flat (small tilt ρ_{macro} of pyrrole groups) with upright phenyls (large dihedral angle θ_{phenyl}; see Table 3). Upon adsorbing on a surface, the phenyls are rotated to adopt a more flat orientation (θ_{phenyl} is decreased) due to attractive interactions with the substrate. This rotation results in a deformation of the macrocycle through steric constraints of the phenyls with the pyrroles.[55] The pyrroles rotate pairwise out of the macrocycle plane; two opposing ones toward the surface (nitrogen points to the surface) and the other two away (nitrogen points toward vacuum). Note that for 2H-TPP/Ag(111) the aminic pyrroles (including the N−H group) rotate down (cf. Figure S1).

Metalation of TPP with 3*d* metals often triggers a flattening of the macrocycle, accompanied by more upright phenyl legs, i.e., a conformation that is more like in the gas phase. Examining the geometric parameters in Table 3, the metalation of 2H-TPP with cerium does not trigger conformational adaptations established for transition metals and moreover changes do not follow the usual phenyl/pyrrole correlation (larger ρ_{macro}, smaller θ_{phenyl}).[56] Instead, the macrocycle is deformed more strongly (second row, larger ρ_{macro}) accompanied by more upright phenyl legs (row 1, larger θ_{phenyl}), not only for the precursor and intermediate, but also for the fully metalated Ce-TPP. This behavior is associated with the lanthanide atomic diameter preventing from a complete macrocycle incorporation. Interestingly, the height $\Delta z_{\text{Ce-s}}$ of the cerium atom above the substrate correlates with the pyrrole tilt angle (cf. rows 2 and 5 in Table 3). The higher the Ce is and the closer it approaches the macrocycle (see $\Delta z_{\text{Ce-m}}$ in row 3), the flatter becomes the latter. Furthermore, $\Delta z_{\text{Ce-s}}$ increases and $\Delta z_{\text{Ce-m}}$ decreases during metalation. This allows the following conclusions for geometric adaptations during the metalation process: The interaction of 2H-TPP with cerium atoms in the precursor complex causes a strong macrocycle distortion that dominates the STM image contrast (see above). Upon coordination, the Ce center is pulled toward the macrocycle and allows for a flatter pyrrole orientation. However, due to its size, it cannot be incorporated fully and hence, the macrocycle can neither flatten out more, as observed for transition metals. Indeed, the final Ce−macrocycle configuration in Ce-TPP/Ag(111) still implies a slightly stronger deformation compared to 2H-TPP/Ag(111) for one of the pyrroles.

DISCUSSION

As noted in the Introduction, for the vast majority of interfacial tetrapyrrole metalation studies 3*d* transition metals were employed. Metalation reactions with other classes of metals such as lanthanides are well-known from solution-based chemistry and were recently explored for ultrathin tetrapyrrole films.[12,13] Unfortunately, the experimental and theoretical results presented above are not fully consistent with a previous interpretation of STM observations.[32] Therein, a distinct species appearing after Ce exposure of a mixed 2H-TPP/Co-TPP matrix on Ag(111) evolved, that is now ascribed to Co-TPP interacting with Ce (cf. Supporting Information, Figure S4), which formation seems to be favorable. Since complexes with the previously reported characteristics were never observed in experiments employing pure 2H-TPP layers, the earlier assignment must be revised (for more details please refer to the Supporting Information). Thus, the present study clarifies the mechanism of on-surface lanthanide tetrapyrrole synthesis in the monolayer regime.

The interaction of Ce atoms with 2H-TPP arrays results in changes within the organic layers that resemble well-documented metalation reactions with transition metals.[3,4,11,24] Namely, the island order is not perturbed, but changes occur at the single-molecule level within the arrays, and the number of modified molecules correlates with the amount of deposited metal. A marked difference to transition metals manifests in the coordination geometry of the final metalloporphyrin and stems from the significantly larger size of the lanthanide. DFT calculations showed that the Ce ion cannot be centered in the inner cavity.[32] Instead it is placed approximately 1 Å out of the macrocycle plane (~1 Å in gas phase calculation, 0.86 Å above the macrocycle for the Ce up configuration and 1.19 Å below the macrocycle for Ce down), i.e., the resulting on-surface complex can exhibit two different arrangements: the Ce atom can be located above or below the macrocycle of TPP, but the direct identification by STM is not straightforward. In the top configuration, the Ce might be detectable by STM if appropriate electronic states are available. Indeed, surface-confined, coordinated Ce atoms and other lanthanides can be imaged as prominent protrusions,[57−60] however there are also examples where lanthanide coordination centers remain hidden in STM images.[57,61−63] For comparison, considering the case of Sn-Pc, the metal center can be positioned above or below the molecular plane, and these two molecular conformations can be reversibly switched.[64−66] By contrast, such characteristics were not observed in our experiments.

Even if the position of the Ce center cannot be determined conclusively in the experiment, the combined STM-DFT analysis clearly signals that the Ce center points toward the Ag(111) substrate. Furthermore, the formation of TPP−Ce−TPP sandwich structures in the TPP (sub-)monolayer regime was only rarely observed and was not reliably reproducible even

DOI: 10.1021/acs.jpcc.7b10363
J. Phys. Chem. C XXXX, XXX, XXX−XXX

at sample temperatures where complexation readily occurs.[12] In order to synthesize $Ce(TPP)_2$ sandwich complexes, cerium has to be evaporated onto TPP thin films.[12] This indicates that the Ce center is located below the porphyrin plane, thus preventing the coordination of an additional tetrapyrrole ligand. This interpretation is in agreement with a report from Katoh et al.,[19] where half-sandwich lanthanide-phthalocyanine (Ln-Pc) derivatives were identified as cracking products in the sublimation of a series of double-decker compounds. The corresponding STM/STS analysis suggests that the lanthanide centers in the observed Ln-Pc (Ln = Tb, Dy, Y) face the employed Au(111) substrate. In agreement, our DFT calculations suggest a definitive energetic preference for an adsorption configuration with the cerium sandwiched between surface and molecule and the simulated images of the Ce down complex exhibit significant similarity to the experiment.

Some metalation reactions do not proceed at room temperature but require elevated temperatures, either to supply metal adatoms (kinetically hindered reaction) or to overcome a formation activation barrier.[4] Since 2H-SAT complexes are well distributed within organic islands, activation energy apparently is needed for the metalation process itself. A notable spectral signature of successful metalation in TPPs and other tetrapyrroles is a LUMO shifted to higher energies.[2,3,11] Indeed, as shown in Figure 2a, the LUMO of the proposed Ce-TPP is upshifted by ≈100 mV corroborating a metalation reaction occurred. Only very few STS data for SAT complexes exist in literature. For comparison, 2H-TPP sitting above a gold atom on Au(111) experiences shifts of 500 mV for both HOMO and LUMO.[29] Following a similar trend for the LUMO, the present 2H-SAT species exhibits an upshift of ≈400 mV. Furthermore, it shows a pronounced peak at −750 mV that is, however, absent for both 2H-TPP and Ce-TPP. Therefore, this feature is tentatively assigned to a mainly metal-derived contribution of Ce states coupling to the silver surface. Indeed, a hybridization of the central metal ion with the Ag(111) can lead to electronic states with characteristic energy.[42,67−69]

The identical features of Ce-induced species following thermal treatment and complexes obtained by STM manipulation allows the following conclusions: (i) The metalation reaction can be triggered both by a voltage pulse from the STM tip or by thermal annealing, (ii) the species with two prominent protrusions (highlighted purple in Figure 1) is indeed the precursor state (2H-SAT) and (iii) the species with only one protrusion is a reaction intermediate, assigned to a 1H-SAT complex. This conclusion is supported by the theoretical evaluation of the energetics of possible species and the calculated STM images. For 2H-TPPs the removal of a hydrogen atom from its macrocycle can manifest as steps in dI/dV spectra and as single and double steps in $I(t)$ traces recorded when applying a voltage pulse to a single 2H-TPP molecule. Hence, it is likely that the steps described in Figure 4d are related to deprotonation, respectively to the redox reaction in the case of metalation. Apparently the reaction pathway includes metastable configurations that might be related to the geometry of SAT complexes. DFT calculations suggest a strong macrocycle deformation causing the hydrogens to point away from the macrocyclic plane, i.e., away from the metal center.[32] The Ce metalation of 2H-TPP layers suggests that the process includes diffusion, intercalation and metalation, and thus exhibits similarities to complexation with transition metals. Moreover, the employment of lanthanides allows clearer identification of precursor and intermediate species. The unambiguous elucidation of the lanthanide−TPP reaction necessitates a reinterpretation of previous results. When depositing Ce onto mixed 2H-/Co-TPP arrays, Ce atoms can intercalate under the array and metalate the free-base species but also bind to Co-TPP, forming Ce−Co-TPP complexes featuring a characteristic electronic signature.

CONCLUSION

In summary, this work presented a detailed experimental and theoretical investigation of the interaction of Ce atoms with surface-confined TPPs. When applying standard protocols known from the metalation of tetrapyrroles with 3*d* transition metals, Ce engages in a metalation reaction to form Ce-TPP. Ce-TPP was comprehensively characterized with STM, (spatially resolved) STS and computational modeling. Interestingly, there is direct evidence for an initial 2H-SAT complex preceding Ce-TPP formation. Furthermore, a 1H-SAT reaction intermediate was identified and characterized directly with submolecular precision. By manipulation experiments the tip-induced on-surface synthesis of intermediate species succeeded, as well as the final Ce-TPP formation from the initial precursor. The real-space analysis, complemented by in-depth theoretical modeling provides insights into the intricate pathways of interfacial lanthanide metalation reactions.

Our study thus contributes to the fundamental understanding of on-surface lanthanide interactions with tetrapyrroles and demonstrates the formation of lanthanide-modified species on surfaces that might provide prospects for heterogeneous catalysis, sensing, quantum engineering, and molecular magnetism.

ASSOCIATED CONTENT

Supporting Information

The Supporting Information is available free of charge on the ACS Publications website at DOI: 10.1021/acs.jpcc.7b10363.

Details on 2H-TPP adsorption on Ag(111), visualization of molecular arrangement of 2H-TPP/Ag(111) employed for DFT modeling, visual summary of energetic results from DFT, and STM and STS data covering the interaction of cerium atoms with mixed Co-TPP/2H-TPP arrays on Ag(111) (PDF)

AUTHOR INFORMATION

Corresponding Author

*(W.A) E-mail: wau@tum.de.

ORCID

Felix Bischoff: 0000-0002-4844-6816

Willi Auwärter: 0000-0001-9452-4662

Ari P. Seitsonen: 0000-0003-4331-0650

Johannes V. Barth: 0000-0002-6270-2150

Author Contributions

The manuscript was written through contributions of all authors. All authors have given approval to the final version of the manuscript.

Notes

The authors declare no competing financial interest.

ACKNOWLEDGMENTS

This work was financially supported by the Munich Center for Advanced Photonics (MAP), TUM-IAS, and the ERC Advanced Grant MolArt (No. 247299). W.A. acknowledges

DOI: 10.1021/acs.jpcc.7b10363
J. Phys. Chem. C XXXX, XXX, XXX−XXX

funding by the DFG via a Heisenberg Professorship. We acknowledge fruitful discussions and experimental support from David Écija. A part of the calculations was performed at Centro Svizzero di Calcolo Scientifico (CSCS), Lugano, under Project uzh11.

REFERENCES

(1) Marbach, H. Surface-Mediated in Situ Metalation of Porphyrins at the Solid−Vacuum Interface. *Acc. Chem. Res.* **2015**, *48*, 2649−2658.
(2) Diller, K.; Papageorgiou, A. C.; Klappenberger, F.; Allegretti, F.; Barth, J. V.; Auwärter, W. In Vacuo Interfacial Tetrapyrrole Metallation. *Chem. Soc. Rev.* **2016**, *45*, 1629−1656.
(3) Auwärter, W.; Écija, D.; Klappenberger, F.; Barth, J. V. Porphyrins at Interfaces. *Nat. Chem.* **2015**, *7*, 105−120.
(4) Gottfried, J. M. Surface Chemistry of Porphyrins and Phthalocyanines. *Surf. Sci. Rep.* **2015**, *70*, 259−379.
(5) Calogero, G.; Bartolotta, A.; Di Marco, G.; Di Carlo, A.; Bonaccorso, F. Vegetable-Based Dye-Sensitized Solar Cells. *Chem. Soc. Rev.* **2015**, *44*, 3244−3294.
(6) Wang, X.-F.; Tamiaki, H. Cyclic Tetrapyrrole Based Molecules for Dye-Sensitized Solar Cells. *Energy Environ. Sci.* **2010**, *3*, 94−106.
(7) Qiao, J.; Liu, Y.; Hong, F.; Zhang, J. A Review of Catalysts for the Electroreduction of Carbon Dioxide to Produce Low-Carbon Fuels. *Chem. Soc. Rev.* **2014**, *43*, 631−675.
(8) Tao, S.; Li, G.; Zhu, H. Metalloporphyrins as Sensing Elements for the Rapid Detection of Trace TNT Vapor. *J. Mater. Chem.* **2006**, *16*, 4521−4528.
(9) Écija, D.; Urgel, J. I.; Seitsonen, A. P.; Auwärter, W.; Barth, J. V. Lanthanide-Directed Assembly of Interfacial Coordination Architectures−from Complex Networks to Functional Nanosystems. *Acc. Chem. Res.* **2018**, DOI: 10.1021/acs.accounts.7b00379.
(10) Gottfried, J. M.; Flechtner, K.; Kretschmann, A.; Lukasczyk, T.; Steinrück, H.-P. Direct Synthesis of a Metalloporphyrin Complex on a Surface. *J. Am. Chem. Soc.* **2006**, *128*, 5644−5645.
(11) Auwärter, W.; Weber-Bargioni, A.; Brink, S.; Riemann, A.; Schiffrin, A.; Ruben, M.; Barth, J. V. Controlled Metalation of Self-Assembled Porphyrin Nanoarrays in Two Dimensions. *ChemPhysChem* **2007**, *8*, 250−254.
(12) Écija, D.; Auwärter, W.; Vijayaraghavan, S.; Seufert, K.; Bischoff, F.; Tashiro, K.; Barth, J. V. Assembly and Manipulation of Rotatable Cerium Porphyrinato Sandwich Complexes on a Surface. *Angew. Chem., Int. Ed.* **2011**, *50*, 3872−3877.
(13) Nardi, M.; Verucchi, R.; Tubino, R.; Iannotta, S. Activation and Control of Organolanthanide Synthesis by Supersonic Molecular Beams: Erbium-Porphyrin Test Case. *Phys. Rev. B: Condens. Matter Mater. Phys.* **2009**, *79*, 125404.
(14) Buchler, J. W.; Decian, A.; Fischer, J.; Kihnbotulinski, M.; Paulus, H.; Weiss, R. Metal Complexes with Tetrapyrrole Ligands. 40. Cerium(Iv) Bis(Octaethylporphyrinate) and Dicerium(III) Tris(Octaethylporphyrinate): Parents of a New Family of Lanthanoid Double-Decker and Triple-Decker Molecules. *J. Am. Chem. Soc.* **1986**, *108*, 3652−3659.
(15) Buchler, J. W.; Kapellmann, H. G.; Knoff, M.; Lay, K. L.; Pfeifer, S. Metal Complexes with Tetrapyrrole Ligands, XXXI. Neutral and Anionoid Bisporphinates of Cerium and Praeseodymium. *Z. Naturforsch., B: J. Chem. Sci.* **1983**, *38*, 1339−1345.
(16) Ishikawa, N.; Sugita, M.; Ishikawa, T.; Koshihara, S.; Kaizu, Y. Lanthanide Double-Decker Complexes Functioning as Magnets at the Single-Molecular Level. *J. Am. Chem. Soc.* **2003**, *125*, 8694−8695.
(17) Ishikawa, N.; Sugita, M.; Ishikawa, T.; Koshihara, S.; Kaizu, Y. Mononuclear Lanthanide Complexes with a Long Magnetization Relaxation Time at High Temperatures: A New Category of Magnets at the Single-Molecular Level. *J. Phys. Chem. B* **2004**, *108*, 11265−11271.
(18) Bogani, L.; Wernsdorfer, W. Molecular Spintronics Using Single-Molecule Magnets. *Nat. Mater.* **2008**, *7*, 179−186.
(19) Katoh, K.; Yoshida, Y.; Yamashita, M.; Miyasaka, H.; Breedlove, B. K.; Kajiwara, T.; Takaishi, S.; Ishikawa, N.; Isshiki, H.; Zhang, Y. F.; et al. Direct Observation of Lanthanide(III)-Phthalocyanine Molecules on Au(111) by Using Scanning Tunneling Microscopy and Scanning Tunneling Spectroscopy and Thin-Film Field-Effect Transistor Properties of Tb(III)- and Dy(III)-Phthalocyanine Molecules. *J. Am. Chem. Soc.* **2009**, *131*, 9967−9976.
(20) Wong, C. P.; Venteicher, Rf; Horrocks, W. D. Lanthanide Porphyrin Complexes - Potential New Class of Nuclear Magnetic-Resonance Dipolar Probe. *J. Am. Chem. Soc.* **1974**, *96*, 7149−7150.
(21) Duchowski, J. K.; Bocian, D. F. Spectroscopic Characterization of Lanthanide Octaethylporphyrin Sandwich Complexes - Effects of Strong π-π-Interaction. *J. Am. Chem. Soc.* **1990**, *112*, 3312−3318.
(22) Müllegger, S.; Tebi, S.; Das, A. K.; Schöfberger, W.; Faschinger, F.; Koch, R. Radio Frequency Scanning Tunneling Spectroscopy for Single-Molecule Spin Resonance. *Phys. Rev. Lett.* **2014**, *113*, 133001.
(23) Cirera, B.; Matarrubia, J.; Kaposi, T.; Gimenez-Agulló, N.; Paszkiewicz, M.; Klappenberger, F.; Otero, R.; Gallego, J. M.; Ballester, P.; Barth, J. V.; et al. Preservation of Electronic Properties of Double-Decker Complexes on Metallic Supports. *Phys. Chem. Chem. Phys.* **2017**, *19*, 8282−8287.
(24) Shubina, T. E.; Marbach, H.; Flechtner, K.; Kretschmann, A.; Jux, N.; Buchner, F.; Steinrück, H.-P.; Clark, T.; Gottfried, J. M. Principle and Mechanism of Direct Porphyrin Metalation: Joint Experimental and Theoretical Investigation. *J. Am. Chem. Soc.* **2007**, *129*, 9476−9483.
(25) Shen, Y.; Ryde, U. Reaction Mechanism of Porphyrin Metallation Studied by Theoretical Methods. *Chem. - Eur. J.* **2005**, *11*, 1549−1564.
(26) Funahashi, S.; Inada, Y.; Inamo, M. Dynamic Study of Metal-Ion Incorporation into Porphyrins Based on the Dynamic Characterization of Metal Ions and on Sitting-Atop Complex Formation. *Anal. Sci.* **2001**, *17*, 917−927.
(27) De Luca, G.; Romeo, A.; Scolaro, L. M.; Ricciardi, G.; Rosa, A. Sitting-Atop Metallo-Porphyrin Complexes: Experimental and Theoretical Investigations on Such Elusive Species. *Inorg. Chem.* **2009**, *48*, 8493−8507.
(28) Li, Y.; Xiao, J.; Shubina, T. E.; Chen, M.; Shi, Z.; Schmid, M.; Steinrück, H.-P.; Gottfried, J. M.; Lin, N. Coordination and Metalation Bifunctionality of Cu with 5,10,15,20-Tetra(4-Pyridyl)Porphyrin: Toward a Mixed-Valence Two-Dimensional Coordination Network. *J. Am. Chem. Soc.* **2012**, *134*, 6401−6408.
(29) Mielke, J.; Hanke, F.; Peters, M. V.; Hecht, S.; Persson, M.; Grill, L. Adatoms Underneath Single Porphyrin Molecules on Au(111). *J. Am. Chem. Soc.* **2015**, *137*, 1844−1849.
(30) Röckert, M.; Franke, M.; Tariq, Q.; Steinrück, H.-P.; Lytken, O. Evidence for a Precursor Adcomplex During the Metalation of 2HTPP with Iron on Ag(1 0 0). *Chem. Phys. Lett.* **2015**, *635*, 60−62.
(31) Doyle, C. M.; Krasnikov, S. A.; Sergeeva, N. N.; Preobrajenski, A. B.; Vinogradov, N. A.; Sergeeva, Y. N.; Senge, M. O.; Cafolla, A. A. Evidence for the Formation of an Intermediate Complex in the Direct Metalation of Tetra(4-Bromophenyl)-Porphyrin on the Cu(111) Surface. *Chem. Commun.* **2011**, *47*, 12134−12136.
(32) Weber-Bargioni, A.; Reichert, J.; Seitsonen, A. P.; Auwärter, W.; Schiffrin, A.; Barth, J. V. Interaction of Cerium Atoms with Surface-Anchored Porphyrin Molecules. *J. Phys. Chem. C* **2008**, *112*, 3453−3455.
(33) Vijayaraghavan, S.; Auwärter, W.; Écija, D.; Seufert, K.; Rusponi, S.; Houwaart, T.; Sautet, P.; Bocquet, M.-L.; Thakur, P.; Stepanow, S.; et al. Restoring the Co Magnetic Moments at Interfacial Co-Porphyrin Arrays by Site-Selective Uptake of Iron. *ACS Nano* **2015**, *9*, 3605−3616.
(34) Auwärter, W.; Schiffrin, A.; Weber-Bargioni, A.; Pennec, Y.; Riemann, A.; Barth, J. V. Molecular Nanoscience and Engineering on Surfaces. *Int. J. Nanotechnol.* **2008**, *5*, 1171.
(35) Createc, D-74391 Erligheim, Germany.
(36) Nečas, D.; Klapetek, P. Gwyddion: An Open-Source Software for Spm Data Analysis. *Open Physics* **2012**, *10*, 181−188.
(37) Hohenberg, P.; Kohn, W. Inhomogeneous Electron Gas. *Phys. Rev.* **1964**, *136*, B864−B871.

DOI: 10.1021/acs.jpcc.7b10363
J. Phys. Chem. C XXXX, XXX, XXX−XXX

(38) Kohn, W.; Sham, L. J. Self-Consistent Equations Including Exchange and Correlation Effects. *Phys. Rev.* **1965**, *140*, A1133−A1138.
(39) Giannozzi, P.; Baroni, S.; Bonini, N.; Calandra, M.; Car, R.; Cavazzoni, C.; Ceresoli, D.; Chiarotti, G. L.; Cococcioni, M.; Dabo, I. Quantum Espresso: A Modular and Open-Source Software Project for Quantum Simulations of Materials. *J. Phys.: Condens. Matter* **2009**, *21*, 395502.
(40) Hamada, I. Van Der Waals Density Functional Made Accurate. *Phys. Rev. B: Condens. Matter Mater. Phys.* **2014**, *89*, 121103.
(41) Dal Corso, A. Pseudopotentials Periodic Table: From H to Pu. *Comput. Mater. Sci.* **2014**, *95*, 337−350.
(42) Auwärter, W.; Seufert, K.; Klappenberger, F.; Reichert, J.; Weber-Bargioni, A.; Verdini, A.; Cvetko, D.; Dell'Angela, M.; Floreano, L.; Cossaro, A.; et al. Site-Specific Electronic and Geometric Interface Structure of Co-Tetraphenyl-Porphyrin Layers on Ag(111). *Phys. Rev. B: Condens. Matter Mater. Phys.* **2010**, *81*, 245403.
(43) Tersoff, J.; Hamann, D. R. Theory of the Scanning Tunneling Microscope. *Phys. Rev. B: Condens. Matter Mater. Phys.* **1985**, *31*, 805−813.
(44) Seufert, K.; Auwärter, W.; García de Abajo, F. J.; Écija, D.; Vijayaraghavan, S.; Joshi, S.; Barth, J. V. Controlled Interaction of Surface Quantum-Well Electronic States. *Nano Lett.* **2013**, *13*, 6130−6135.
(45) Buchner, F.; Kellner, I.; Hieringer, W.; Görling, A.; Steinrück, H.-P.; Marbach, H. Ordering Aspects and Intramolecular Conformation of Tetraphenylporphyrins on Ag(111). *Phys. Chem. Chem. Phys.* **2010**, *12*, 13082−13090.
(46) Rojas, G.; Chen, X.; Bravo, C.; Kim, J.-H.; Kim, J.-S.; Xiao, J.; Dowben, P. A.; Gao, Y.; Zeng, X. C.; Choe, W.; et al. Self-Assembly and Properties of Nonmetalated Tetraphenyl-Porphyrin on Metal Substrates. *J. Phys. Chem. C* **2010**, *114*, 9408−9415.
(47) Rojas, G.; Simpson, S.; Chen, X.; Kunkel, D. A.; Nitz, J.; Xiao, J.; Dowben, P. A.; Zurek, E.; Enders, A. Surface State Engineering of Molecule−Molecule Interactions. *Phys. Chem. Chem. Phys.* **2012**, *14*, 4971.
(48) Auwärter, W.; Seufert, K.; Bischoff, F.; Écija, D.; Vijayaraghavan, S.; Joshi, S.; Klappenberger, F.; Samudrala, N.; Barth, J. V. A Surface-Anchored Molecular Four-Level Conductance Switch Based on Single Proton Transfer. *Nat. Nanotechnol.* **2012**, *7*, 41−46.
(49) Hennig, J.; Limbach, H. H. Kinetic Study of Hydrogen Tunnelling in Meso-Tetraphenylporphine by Nuclear Magnetic Resonance Lineshape Analysis and Selective T1ρ- Relaxation Time Measurements. *J. Chem. Soc., Faraday Trans. 2* **1979**, *75*, 752−766.
(50) Limbach, H. H.; Hennig, J. Quasiclassical Calculations of One-Dimensional Potential Parameters of the Hydrogen Migration in Meso-Tetraphenylporphine from Experimental Tunnel Rates. *J. Chem. Phys.* **1979**, *71*, 3120−3124.
(51) Liljeroth, P.; Repp, J.; Meyer, G. Current-Induced Hydrogen Tautomerization and Conductance Switching of Naphthalocyanine Molecules. *Science* **2007**, *317*, 1203−1206.
(52) Garnica, M.; Schwarz, M.; Ducke, J.; He, Y.; Bischoff, F.; Barth, J. V.; Auwärter, W.; Stradi, D. Comparative Study of the Interfaces of Graphene and Hexagonal Boron Nitride with Silver. *Phys. Rev. B: Condens. Matter Mater. Phys.* **2016**, *94*, 155431.
(53) Comanici, K.; Buchner, F.; Flechtner, K.; Lukasczyk, T.; Gottfried, J. M.; Steinrück, H.-P.; Marbach, H. Understanding the Contrast Mechanism in Scanning Tunneling Microscopy (STM) Images of an Intermixed Tetraphenylporphyrin Layer on Ag(111). *Langmuir* **2008**, *24*, 1897−1901.
(54) Kumagai, T.; Hanke, F.; Gawinkowski, S.; Sharp, J.; Kotsis, K.; Waluk, J.; Persson, M.; Grill, L. Controlling Intramolecular Hydrogen Transfer in a Porphycene Molecule with Single Atoms or Molecules Located Nearby. *Nat. Chem.* **2014**, *6*, 41−46.
(55) Wölfle, T.; Görling, A.; Hieringer, W. Conformational Flexibility of Metalloporphyrins Studied by Density-Functional Calculations. *Phys. Chem. Chem. Phys.* **2008**, *10*, 5739−5742.
(56) Diller, K.; Klappenberger, F.; Marschall, M.; Hermann, K.; Nefedov, A.; Wöll, Ch.; Barth, J. V. Self-Metalation of 2H-Tetraphenylporphyrin on Cu(111): An X-Ray Spectroscopy Study. *J. Chem. Phys.* **2012**, *136*, 014705.
(57) Cirera, B.; Dordević, L.; Otero, R.; Gallego, J. M.; Bonifazi, D.; Miranda, R.; Écija, D. Dysprosium-Carboxylate Nanomeshes with Tunable Cavity Size and Assembly Motif through Ionic Interactions. *Chem. Commun.* **2016**, *52*, 11227−11230.
(58) Écija, D.; Urgel, J. I.; Papageorgiou, A. C.; Joshi, S.; Auwärter, W.; Seitsonen, A. P.; Klyatskaya, S.; Ruben, M.; Fischer, S.; Vijayaraghavan, S.; et al. Five-Vertex Archimedean Surface Tessellation by Lanthanide-Directed Molecular Self-Assembly. *Proc. Natl. Acad. Sci. U. S. A.* **2013**, *110*, 6678−6681.
(59) Urgel, J. I.; Écija, D.; Auwärter, W.; Barth, J. V. Controlled Manipulation of Gadolinium-Coordinated Supramolecules by Low-Temperature Scanning Tunneling Microscopy. *Nano Lett.* **2014**, *14*, 1369−1373.
(60) Urgel, J. I.; Écija, D.; Auwärter, W.; Papageorgiou, A. C.; Seitsonen, A. P.; Vijayaraghavan, S.; Joshi, S.; Fischer, S.; Reichert, J.; Barth, J. V. Five-Vertex Lanthanide Coordination on Surfaces: A Route to Sophisticated Nanoarchitectures and Tessellations. *J. Phys. Chem. C* **2014**, *118*, 12908−12915.
(61) Lyu, G.; Zhang, Q.; Urgel, J. I.; Kuang, G.; Auwärter, W.; Écija, D.; Barth, J. V.; Lin, N. Tunable Lanthanide-Directed Metallosupramolecular Networks by Exploiting Coordinative Flexibility through Ligand Stoichiometry. *Chem. Commun.* **2016**, *52*, 1618−1621.
(62) Urgel, J. I.; Cirera, B.; Wang, Y.; Auwärter, W.; Otero, R.; Gallego, J. M.; Alcamí, M.; Klyatskaya, S.; Ruben, M.; Martín, F.; et al. Surface-Supported Robust 2D Lanthanide-Carboxylate Coordination Networks. *Small* **2015**, *11*, 6358−6364.
(63) Urgel, J. I.; Écija, D.; Lyu, G.; Zhang, R.; Palma, C. A.; Auwärter, W.; Lin, N.; Barth, J. V. Quasicrystallinity Expressed in Two-Dimensional Coordination Networks. *Nat. Chem.* **2016**, *8*, 657−662.
(64) Wang, Y. F.; Kröger, J.; Berndt, R.; Hofer, W. A. Pushing and Pulling a Sn Ion through an Adsorbed Phthalocyanine Molecule. *J. Am. Chem. Soc.* **2009**, *131*, 3639−3643.
(65) Stadler, C.; Hansen, S.; Kröger, I.; Kumpf, C.; Umbach, E. Tuning Intermolecular Interaction in Long-Range-Ordered Submonolayer Organic Films. *Nat. Phys.* **2009**, *5*, 153−158.
(66) Baran, J. D.; Larsson, J. A. Structure and Energetics of Shuttlecock-Shaped Tin-Phthalocyanine on Ag(111): A Density Functional Study Employing Dispersion Correction. *J. Phys. Chem. C* **2012**, *116*, 9487−9497.
(67) Flechtner, K.; Kretschmann, A.; Steinrück, H.-P.; Gottfried, J. M. NO-Induced Reversible Switching of the Electronic Interaction between a Porphyrin-Coordinated Cobalt Ion and a Silver Surface. *J. Am. Chem. Soc.* **2007**, *129*, 12110−12111.
(68) Hieringer, W.; Flechtner, K.; Kretschmann, A.; Seufert, K.; Auwärter, W.; Barth, J. V.; Görling, A.; Steinrück, H.-P.; Gottfried, J. M. The Surface Trans Effect: Influence of Axial Ligands on the Surface Chemical Bonds of Adsorbed Metalloporphyrins. *J. Am. Chem. Soc.* **2011**, *133*, 6206−6222.
(69) Liao, M.-S.; Scheiner, S. Electronic Structure and Bonding in Metal Porphyrins, Metal = Fe, Co, Ni, Cu, Zn. *J. Chem. Phys.* **2002**, *117*, 205−219.

DOI: 10.1021/acs.jpcc.7b10363
J. Phys. Chem. C XXXX, XXX, XXX−XXX